Analytica Chimica Acta 1277 (2023) 341634

Contents lists available at ScienceDirect

Analytica Chimica Acta

journal homepage: www.elsevier.com/locate/aca

Capillary flow-driven immunoassay platform for COVID-19 antigen diagnostics

Jeremy S. Link [a,1], Cody S. Carrell [a,1], Ilhoon Jang [a,b,1], Elijah J.O. Barstis [a], Zachary D. Call [a], Rae A. Bellows [a], John J. O'Donnell-Sloan [a], James S. Terry [c], Loran B.R. Anderson [c], Yosita Panraksa [c,d], Brian J. Geiss [c,f], David S. Dandy [e,f], Charles S. Henry [a,e,f,g,*]

[a] Department of Chemistry, Colorado State University, USA
[b] Institute of Nano Science and Technology, Hanyang University, South Korea
[c] Department of Microbiology, Immunology and Pathology, Colorado State University, USA
[d] Myobacteria Research Laboratories, Colorado State University, USA
[e] Department of Chemical and Biological Engineering, Colorado State University, USA
[f] School of Biomedical Engineering, Colorado State University, USA
[g] Metallurgy and Materials Research Institute, Chulalongkorn University, Bangkok, Thailand

HIGHLIGHTS

- Developed a device that steps of a traditional ELISA from 1 user step.
- Device detects SARS-CoV-2 nucleocapsid protein at similar LOD to an ELISA.
- Able to visually detect clinically relevant levels of SARS-CoV-2 in 20 min.
- Aspects of the device can be adjusted to detect other diseases.

GRAPHICAL ABSTRACT

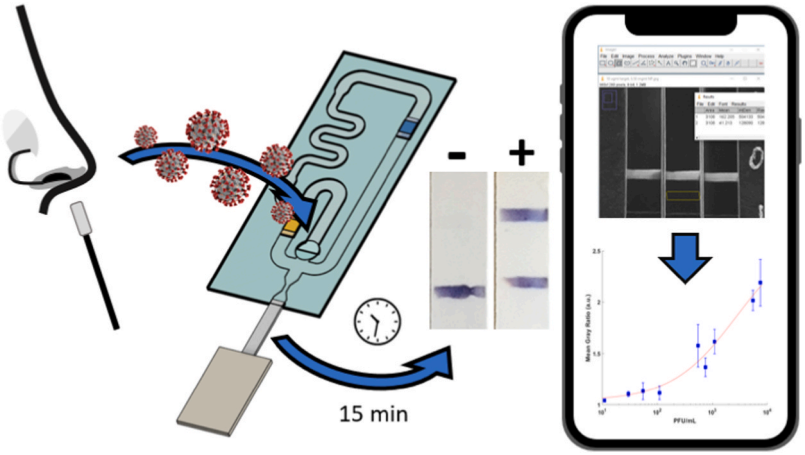

ARTICLE INFO

Keywords:
COVID-19
SARS-CoV-2
Point-of-care
Capillary-driven microfluidics

ABSTRACT

Over the last few years, the SARS-CoV-2 pandemic has made the need for rapid, affordable diagnostics more compelling than ever. While traditional laboratory diagnostics like PCR and well-plate ELISA are sensitive and specific, they can be costly and take hours to complete. Diagnostic tests that can be used at the point-of-care or at home, like lateral flow assays (LFAs) are a simple, rapid alternative, but many commercially available LFAs have been criticized for their lack of sensitivity compared to laboratory methods like well-plate ELISAs. The Capillary-

* Corresponding author. Department of Chemistry, Colorado State University, USA.
E-mail address: chuck.henry@colostate.edu (C.S. Henry).
[1] These authors contributed equally to this work.

https://doi.org/10.1016/j.aca.2023.341634
Received 21 April 2023; Received in revised form 14 July 2023; Accepted 15 July 2023
Available online 27 July 2023

Diagnostic testing
Immunoassays

Driven Immunoassay (CaDI) device described in this work uses microfluidic channels and capillary action to passively automate the steps of a traditional well-plate ELISA for visual read out. This work builds on prior capillary-flow devices by further simplifying operation and use of colorimetric detection. Upon adding sample, an enzyme-conjugated secondary antibody, wash steps, and substrate are sequentially delivered to test and control lines on a nitrocellulose strip generating a colorimetric response. The end user can visually detect SARS-CoV-2 antigen in 15–20 min by naked eye, or results can be quantified using a smartphone and software such as ImageJ. An analytical detection limit of 83 PFU/mL for SARS-CoV-2 was determined for virus in buffer, and 222 PFU/mL for virus spiked into nasal swabs using image analysis, similar to the LODs determined by traditional well-plate ELISA. Additionally, a visual detection limit of 100 PFU/mL was determined in contrived nasal swab samples by polling 20 untrained end-users. While the CaDI device was used for detecting clinically relevant levels of SARS-CoV-2 in this study, the CaDI device can be easily adapted to other immunoassay applications by changing the reagents and antibodies.

1. Introduction

SARS-CoV-2, the causative agent of COVID-19, is most infectious directly before and after the onset of symptoms [1]. Studies have shown that viral load in the respiratory tract of patients peaks within the first week of symptom onset [2]; however, because viral shedding can occur before symptom onset, it has been argued that symptomatic and pre--symptomatic spread are large contributors to rapid pathogen transmission [3]. For this reason, one of the most important tools to diagnose COVID-19 and other contagious diseases is readily available, affordable, and rapid [4]. The ideal diagnostic would be operational outside of a clinical laboratory, have high clinical specificity and sensitivity (i.e., good positive and negative predictive values), be simple enough for average untrained users to operate, and fast enough to obtain meaningful results (<15 min). Unfortunately, most commercial SARS-CoV-2 diagnostics do not meet one or more of these standards [5–7].

Quantitative polymerase chain reaction (qPCR) is the most common method used to detect SARS-CoV-2. qPCR methods have been shown to detect both genomic and subgenomic RNA. While genomic RNA would be a good indication that viable, transmittable virus is still present in a patient, subgenomic RNA may be remnants of inactive virus that remain in the nose or pharynx after a patient is no longer contagious [2,8]. Consequently, work by Alexandersen et al. showed that qPCR can return a positive result up to 17 days after symptom onset when an individual is no longer infectious, arguing that PCR targeting subgenomic RNA may have some crucial faults as a diagnostic method [8]. Furthermore, qPCR requires expensive instruments, trained technicians, and several hours to run *after* the time it takes to transport sample to a laboratory. For these reasons, frequent, affordable, testing has been advocated for over infrequent but sensitive qPCR [9–12]. Rapid testing offering qualitative, yes/no results in less than 30 min would dramatically increase the number of tests performed while providing actionable results. Assays that target antigen detection rather than RNA amplification offer a compromise between sensitivity and practicality and are available in several formats including laboratory-based enzyme linked immunosorbent assays (ELISA) and lateral flow assays (LFAs) [5].

Well-plate ELISA offers higher sensitivity and specificity than LFAs, but, like qPCR, requires expensive instrumentation and trained technicians, making rapid, point-of-care and at-home testing difficult to impossible [13]. LFAs are user-friendly, affordable, and offer results in ~15 min. However, the improvements in ease-of-use relative to laboratory tests come at the cost of performance. Rapid antigen LFAs for SARS-CoV-2 have shown decent performance in controlled settings and much poorer in actual clinical validations [14–17]. For example, Cubas-Atienzar et al. found that only 4/19 rapid antigen tests maintained a limit of detection below the World Health Organization's suggestion of 500 PFU/mL when using dry nasal swabs [16]. Additionally, many tests meet the sensitivity requirements only when a patient has a high viral load, but struggle to maintain their sensitivity otherwise [18–20]. Therefore, an urgent need still exists for a diagnostic with the analytical performance of a laboratory-based ELISA and the ease-of-use of an LFA.

Well-plate ELISAs outperform LFAs for several reasons, but their superior sensitivity stems from the ability to use an enzyme/substrate reaction as a label instead of a gold nanoparticle. LFAs cannot use enzyme labels because they lack the ability to sequentially add and wash reagents from the test zone. Paper-based ELISAs have been developed to lower some of the barriers imposed by traditional well plate ELISAs. Many early paper-based ELISAs simply swap a microwell plate with paper wells, but this alternative still leaves complicated procedures and inferior detection limits [21–23]. Developments to simplify assay operations have been applied to SARS-CoV-2 antigen and antibody detection. For example, vertical flow assays have been made for *N*-protein and antibodies against *N*-protein. However, as is the case with many paper-based ELISAs, background and signal in the blanks are inevitable without incorporating additional washing steps [24,25]. Microfluidic devices designed to automate the reagent delivery and washing steps associated with an ELISA exist, but often require multiple steps, lack simplicity and portability, or are too complicated for minimally trained end-users. Table S1 highlights several of these technologies [26–31]. Included are devices that perform enzyme-labeled sandwich immunoassays without the need for a powered instrument, although some use complicated designs and manufacturing techniques [32,33]. Capillary-driven devices have been used for decades in traditional microfluidic systems; however, the most often rely relatively complicated or expensive manufacturing techniques like photolithography or 3D printing [34,35]. Electrowetting-on-dielectric (EWOD) and centrifugal microfluidic devices have also been developed for sequential delivery of reagents, however they encounter some of the same drawbacks as mentioned above: complicated and expensive manufacturing, reliance on a power source, and complicated assay procedures [36–40]. Sequential steps in capillary driven devices have been previously demonstrated, but often fail to demonstrate efficient washing between reagent addition steps [41–45]. Instead, they use gold-enhancement reagents to improve the signal of traditional nanoparticle-based assays instead of enzyme/substrate amplification, which requires much more stringent washing to avoid background noise [41–45].

In this work, we describe the colorimetric and visual detection of SARS-CoV-2 nucleocapsid protein using a microfluidic device that fully automates the reagent delivery and washing steps of an ELISA while retaining the simplicity of an LFA. Using capillary-driven microfluidics discussed previously [46–50], the capillary-driven immunoassay (CaDI) device sequentially delivers sample, reagents, and wash buffer to a nitrocellulose test zone to perform an enzymatic sandwich immunoassay with a visual readout. Previous published iterations of the CaDI device use electrochemical detection to quantify signal for clinically relevant levels of SARS-CoV-2 [51]. While the CaDI device, both in the previous paper and this work, is made of affordable materials, electrochemical detection relies on expensive potentiostat to detect signal. While more portable, affordable potentiostats that rely on smartphones and near-field communication technologies are being developed to mitigate this cost [51,52], visual detection remains the simplest and most user-friendly form of POC or at-home testing for qualitative, positive/-negative results. These benefits become especially important in

low-resource or rural areas. Fluorescently labeled antibodies or enzyme/substrate products could also be considered as a sensitive alternative to visual detection, it also relies on imaging equipment and an external excitation source, reducing its accessibility. In this work, a nitrocellulose test strip is connected to the outlet of the device, and a waste pad is used to draw buffer and reagents through the nitrocellulose. The channels in the CaDI device supply power-free capillary flow, resulting in efficient washing of the test zone, increased reagent delivery, and 15–20 min assay times. Results can be read by eye for a positive/negative answer, or a smart phone image can be analyzed for quantitative results, further simplifying detection methods compared previous iterations of the device.

We previously demonstrated similar devices to the CaDI device used to colorimetrically detect SARs-CoV-2 antibodies from whole human blood as well as the tuberculosis marker, Lipoarabinomannan (LAM) [53,54]. While antibody detection gives information on a person's level of immunity, it does not diagnose active infections. Likewise, the LAM detection system used urine samples and required multiple steps for operation. Here, we demonstrate the CaDI's ability to detect SARS-CoV-2 nucleocapsid protein (*N*-protein) from inactivated SARS-CoV-2 virus spiked in buffer and in nasal swab samples. The device operates with a single sample addition step, maintaining the simplicity of a LFA while incorporating enzyme/substrate signal amplification to produce a visual, colored product. With this device, a detection limit of 83 PFU/mL was obtained for inactivated SARS-CoV-2 in buffer, only one order of magnitude above the limit of detection (LOD) for a traditional well-plate ELISA run with the same reagents. Nasal swabs were collected and spiked with inactivated virus; for these contrived samples, an analytical detection limit of 222 PFU/mL was determined. To stress the importance and application of visual detection, a visual LOD study was also performed. Contrived nasal swab samples were run at varying concentrations, and the FDA visual LOD protocol was followed to determine a visual LOD of 100 PFU/mL. Beyond the SARs-CoV-2 assays demonstrated in this and previous work, the CaDI device can be used for a multitude of point-of-care immunoassays. Due to its low cost of materials (roughly $1.66/device, Table S2) and simplicity the device represents a major step forward in providing high quality diagnostics in at-home and resource limited settings. The CaDI device bridges the gap between the easy-to-operate LFA and the high-performing laboratory standard ELISA.

2. Materials and methods

Device assembly: The CaDI device was made of alternating layers of transparency film (3M™ 9984, Saint Paul, MN, USA) and double-sided adhesive (3M™ 467 MP, Saint Paul, MN, USA). The channels in each layer were cut under a flow of nitrogen gas with a CO_2 laser cutter (Epilog Zing, Golden, CO, USA) and laminated together using a temperature controlled TruLam laminator at room temperature. The channel designs and dimensions are shown in Figure S1. The first four layers were stacked and laminated. The reagent pads were then added to the channels, followed by the final layer of patterned 9984 film. Finally, the nitrocellulose test strip (FF80HP Plus, Cytiva, Marlborough, MA, USA) was inserted to the outlet of the device and an absorbent material (CFSP223000, MilliporeSigma Burlington, MA, USA) was placed on the end of the nitrocellulose and secured with adhesive (3M™ 468 MP, Saint Paul, MN, USA). To demonstrate sequential delivery and washing in the device (Fig. 2A), tartrazine (yellow dye, 1870 μM) and erioglaucine (blue dye, 800 μM) were dried onto reagent pads [47].

Reagent pad preparation: The reagent pads were made from a glass fiber conjugate release pad (GFDX203000, MilliporeSigma Burlington, MA, USA) pretreated by immersing in a blocking solution of 10 mM PBS (Thermo Scientific, Rockford, IL, USA), 3% sucrose, 0.5% Tween-20, and 0.1% thimerosal (MilliporeSigma) for 15 min. The pads were removed from the blocking solution, dried overnight at 37 °C, and cut into 3 × 5 mm^2 rectangles by hand with a razor blade. The reagent pads containing the enzyme-conjugated secondary antibody were further blocked with 15 μL of 0.57% casein (MilliporeSigma) dissolved in 50 mM borate buffer per pad and dried for 30–45 min at 37 °C. After drying, 5 μL of detection antibody labeled with horseradish peroxidase (2°Ab-HRP) was pipetted onto the casein-blocked pad (40,143-MM05-H, Sino Biological, Beijing, China) and dried for 30 min at 37 °C. The 2°Ab-HRP was diluted in a stabilizing, long-term storage buffer consisting of 0.01 M ethylenediaminetetraacetic acid, 0.01 M $FeSO_4$, 4% trehalose, and 0.1% BSA in PBS, before adding to the pad [55]. 3,3′,5,5′-tetramethylbenzidine solution (TMBM-0100-01, Surmodics Inc., Eden Prairie, MN, USA) was pipetted onto the second reagent pad in 3 separate 7.5 μL aliquots, allowing the pad to dry for 5–7 min at 37 °C between additions. After the final TMB addition both reagent pads were dried for 120 min at 37 °C before added to the CaDI device. Devices were used immediately after assembling or briefly stored in mylar bags with desiccant pouches.

Nitrocellulose: The nitrocellulose test strip (FF80HP Plus, Cytiva, Marlborough, MA, USA) was striped with a control and test line using a BioSpot reagent printer (BioFluidix, Breisgau, Germany). The control line was striped with a SARS-CoV-2 *N*-protein at 0.25 mg/mL (40,143-V08B, Sino Biological) in a solution of 20 mM Tris, 500 mM NaCl, 10% glycerol, pH 7.4, 5%–8% trehalose, mannitol and 0.01% Tween 80. The test line was striped with a monoclonal *anti*-SARS-CoV-2 *N*-protein at 0.88 mg/mL (40,143-MM08, Sino Biological). The test line striping solution contained trehalose (Calbiochem, San Diego, CA USA) and glycerol (Mallinckrodt, Dublin, Ireland) with final concentration of 45 mM and 4.5% respectively to increase stability of the protein during drying. After striping, the nitrocellulose was dried overnight in a desiccator and blocked with Stabilguard™ (SG01-1000, Surmodics Inc.) by allowing it to wick through the membrane from bottom to top until the membrane was fully saturated. The nitrocellulose was then dried again for 5 h at 37 °C before cutting into 3 × 15 mm^2 strips with the laser cutter and stored at 4 °C with desiccant pouches until use.

Assay operation: The extraction/running buffer was made of a 1.5× stable peroxide buffer (Thermo Fisher, 34,062) buffered to pH 6.5 with sodium hydroxide. 150 mM sodium chloride was added as well as 0.1% Igepal CA630 (Fisher Scientific) and 0.1% Tween-20 to lyse/inactivate the virus and reduce non-specific adsorption in the device. Inactivated SARS-CoV-2 virus (USA-WA1/2020) was prepared and quantified by plaque assay as previously described [56]. Inactivated virus was spiked into extraction buffer at the desired concentration before 100 μL of sample was added to the sample inlet on the CaDI device to begin the assay. For experiments requiring nasal swab samples, an anterior nares swab (FoamTec Medical, MP1301AST) was collected under approval of the IRB board of Colorado State University by swabbing the inside of the nostril with three rotations of the swab in each nostril. For spiked swab samples, 50 μL of inactivated virus sample was added to the swab after collection. The swabs were submerged in 300 μL of extraction buffer, swirled for 15 s, pulled into a syringe and filtered with a 0.2 μm PTFE syringe filter (Fisher, 13-1001-14), and 100 μL of the filtered sample was added to the device to begin the assay. The workflow for nasal swab samples can be seen in Fig. 1.

The 100 μL of extraction buffer provides the washing buffer, target analyte, and H_2O_2, while the CaDI device supplies all other reagents, so no further end user input is required. The assay is finished once the channel above the substrate reagent pad is emptied, which takes 15–20 min (Videos S1). The nitrocellulose strip was then allowed to dry at room temperature for 5 min before imaging for analysis.

Image/Data Analysis: After an assay was complete, the nitrocellulose was removed, dried, and placed on a white background in a light box containing 16 LEDs for consistent lighting [57,58]. Images were captured using a Motorola One smartphone. NIH ImageJ software was used for analysis. Images were inverted, converted to 8-bit greyscale, and the area around the test line was surrounded using the polygon tool. The mean gray value was taken for the selected area at the test line and directly below the test line. The ratio of the two values (test line/-background) is the "mean gray ratio," and helps account for slight

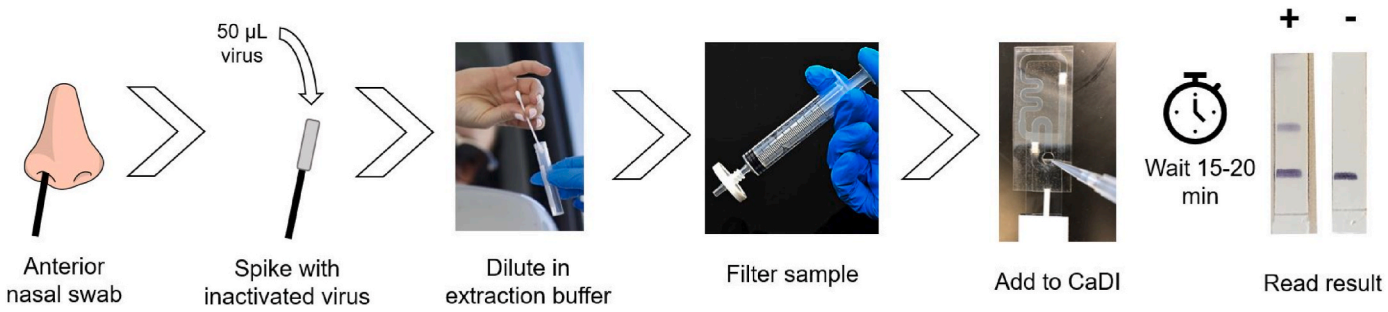

Fig. 1. The workflow for nasal swab samples is shown above. After a swab is collected, it is submerged in extraction buffer to lyse any virus present. The buffer/sample is then pushed through a syringe filter before adding to the device.

differences in lighting/background between images. The mean gray ratio was used as the signal to quantify the color change at the test line.

2.1. Visual LOD

For the visual limit of detection, a variation of methods from FDA emergency use authorization approved devices was used [59]. CaDI devices were run (n = 1) at varying concentrations (0, 50, 100, 200, 300, 400, 500 PFU/mL) of inactivated virus following the nasal swab assay operation as previously described. First, an anterior nasal swab was collected by swabbing inside both nostrils, 3 rotations in each. 50 µL of inactivated virus sample was then added to the swab after collection. The swabs were submerged in 300 µL of extraction buffer, swirled for 15 s, filtered with a 0.2 mm PTFE syringe filter (Fisher, 13-1001-14), and 100 µL of the filtered sample was added to the device to begin the assay. The nitrocellulose test strip was removed from the device, placed into a small Petri dish, and randomly assigned a letter between A and G.

Twenty untrained volunteers were recruited and informed that two lines present on the nitrocellulose membrane indicated a positive test, while a single line indicated a negative test. They were instructed to look at each of seven nitrocellulose test strips and to identify each strip as positive or negative. Responses for each nitrocellulose test strip were recorded.

2.2. Well-plate ELISA

50 µL of 40,143-MM08 (1 µg/mL diluted in 10 mM PBS, pH 7.2, along with 45 mM trehalose and 4.5% glycerol) was added to each well in a Corning™ Costar® 96-well assay plate and allowed to adsorb overnight at 4 °C while shaking. Each well in the plate was then washed three times with 200 µL of wash buffer (10 mM PBS containing 0.1% Tween-20). After washing, wells were blocked with 200 µL

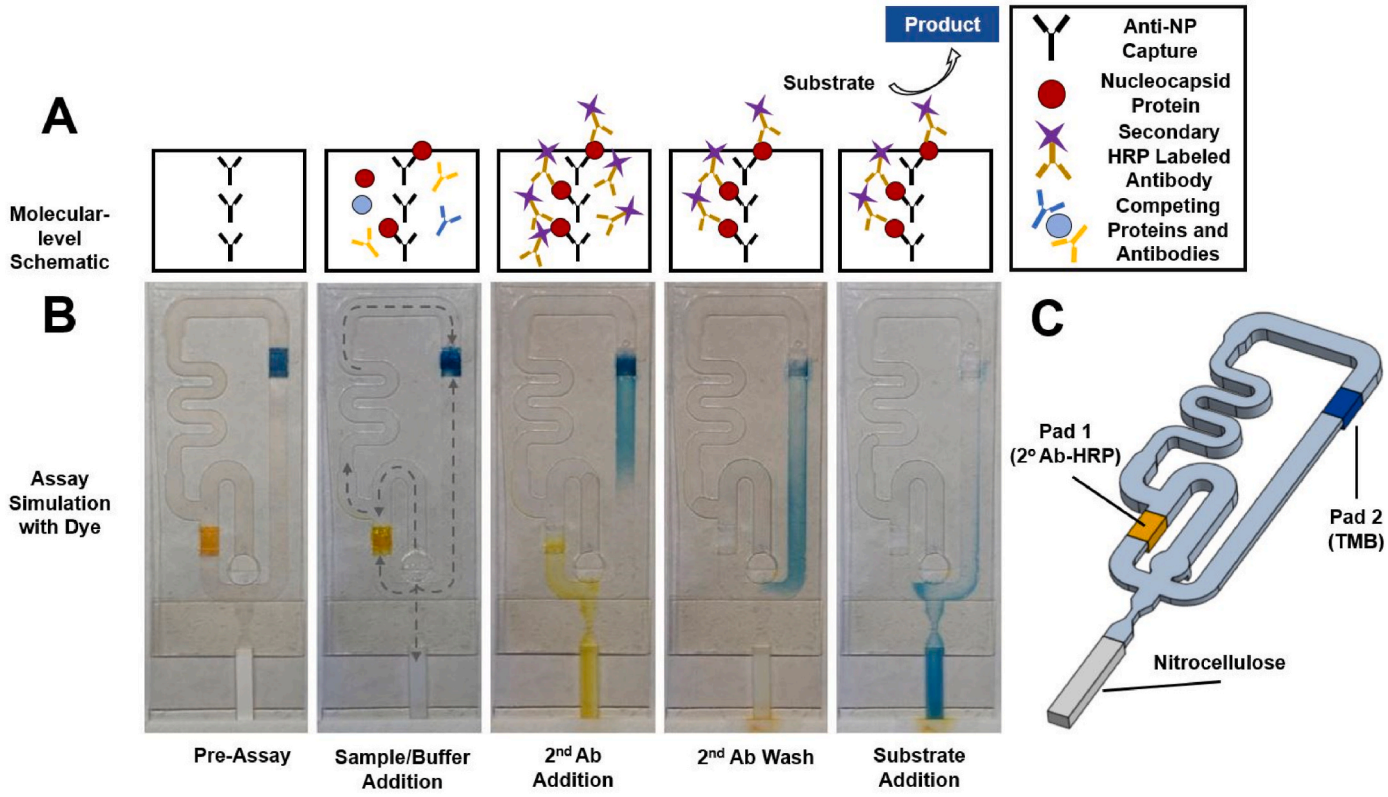

Fig. 2. (A) Molecular level representation of the immunoassay steps at the test line of the nitrocellulose membrane using an HRP-labeled antibody. The steps shown here occur at the test line on the nitrocellulose and correspond to the steps simulated with dye in B (B) Simulation of reagent addition and washing steps using yellow food dye to represent the HRP-antibody and blue food dye to represent the TMB substrate. (C) 3D rendering of the CaDI device channels that show how each plug of buffer in the channels is used in the assay. To see the assay and sequential delivery, refer to video S1 and video S2. (For interpretation of the references to color in this figure legend, the reader is referred to the Web version of this article.)

StabilGuard™ Immunoassay Stabilizer for 1 h at 37 °C while shaking. After an additional 3 washes, 50 μL of varying concentrations of inactivated SARS-CoV-2 virus (diluted in extraction buffer with varying conditions described in the supplemental section) was added to the wells and allowed to incubate for 1 h at ambient temperature while shaking. Each well was washed three times, and 50 μL of 40,143-MM05 (0.5 μg/mL diluted in drying buffer described above) was then added to each well and incubated for 1 h at ambient temperature while shaking. After a final three washes, 50 μL of 1-Step™ Ultra TMB-ELISA was added to each well and allowed to react for 2.5 min. This reaction was then stopped by adding 50 μL of 1 M H_2SO_4 to each well and read at OD 450 nm with a PerkinElmer VICTOR™ ×5 2030 Multilabel plate reader.

3. Results/discussion

Sequential delivery and washing: The sequential flow and reagent delivery in the CaDI device has been described in previous work with electrochemical detection [51]. The gray arrows in Fig. 2B show the direction in which the channels fill from after sample is added to the sample inlet. The nitrocellulose is wetted by the sample, after which all fluid in the CaDI device flows into the waste pad through the nitrocellulose via capillary action.

N-protein in the sample binds to a capture antibody at the test line of the nitrocellulose. Dried reagents (represented by blue and yellow dye in Fig. 2B) are rehydrated and sequentially flow through the nitrocellulose and across the test and control lines. 2°Ab-HRP (represented by the yellow dye in Fig. 2B) to the test line where it binds to the target, followed by as plug of buffer to wash excess 2°Ab-HRP from the nitrocellulose. Lastly, substrate (represented with blue dye in Fig. 2B) passes through the nitrocellulose, reacting with enzyme present at the test and control lines. There is *N*-protein in the buffer that will bind to 2°Ab-HRP in the conjugate release pad; however, in this study this did not lead to a noticeable hook effect. The order of flow is determined depending on the channel height and geometry. For example, the channel directly under the substrate pad (blue pad in Fig. 2B) is created with a single layer of double-sided adhesive removed to create depth (~60 μm). The channel above the substrate pad is made by removing two layers of double-sided adhesive and one layer of transparency film (~220 μm). The channel dimensions and depths can be seen more clearly in Figure S1.

In traditional ELISAs, washing the well several times with 200–500 μL of buffer is required before adding the substrate to minimize background and/or false positives. These washing steps help improve sensitivity and specificity but add time and complexity [60,61]. Thorough washing is difficult in LFAs because the buffer flows linearly through the LFA without any separation of steps by flow. The washing step in a CaDI device is performed using the buffer occupying the channel between pad 2 and the nitrocellulose membrane. This wash step is critical for removing any excess 2°Ab-HRP from the test line, preventing false positives, and is especially important for visual readouts where untrained end-users may be asked to interpret results. The serpentine pattern in the left-most channel was added to ensure that the buffer from both channels meet at the TMB pad at similar times, preventing air bubbles from stopping flow. The pinched channel near the nitrocellulose was implemented in an attempt to enhance passive mixing [62], ensuring that the 2°Ab-HRP and TMB cover the nitrocellulose evenly as they flow through.

Enzyme-substrate system. The next consideration for the CaDI antigen assay was the choice of enzyme and substrate. With a single sample addition step, all washing, binding, and enzymatic reaction steps must occur under the same conditions. Each of these steps has its own optimal operating conditions, so determining assay parameters that can work for the entire assay was critical. Horseradish peroxidase (HRP) was chosen for this application because it is stable and active at physiological pH and has several colorimetric substrates that can be used for naked-eye detection. Of these substrates, 3,3′,5,5′-tetramethylbenzidine (TMB) was chosen. Oxidized TMB is soluble and would be washed through the nitrocellulose after reacting with HRP and H_2O_2 under normal conditions. However, the commercially available TMB blotting solution used in our device contains additives that form an insoluble product, leaving a dark blue precipitate and requiring no "stop solution" for the reaction.

Immunoassay optimization. Immunoassays are highly dependent on the specificity and binding efficiency of the antibodies. An extensive report on commercially available antibodies for SARS-CoV-2 *N*-protein detection was published in 2021, and the results from that study were used to guide the antibody selection in this work [63]. Five Sino Biological antibodies were chosen for screening in the CaDI devices (Figure S3 and S4), and 40,413-MM05 and 40,413-MM08 were chosen as the detection and capture antibodies respectively as a result. In previous work with electrochemical detection of SARS-CoV-2, this antibody pair was also used and tested against a range of interferents, resulting in excellent specificity [51]. To determine optimal buffer conditions, a traditional well-plate ELISA was performed under different buffer conditions as described in the methods section (Figure S5). The extraction buffer at pH 6.5 and 150 mM NaCl was comparable to buffer at pH 7.4 and 225 mM NaCl. However, the optimal pH for antibody binding is ~7.2, and the optimal pH for HRP activity is ~5.5. Since it lies in between that pH range, buffer containing 150 mM NaCl at pH 6.5 was chosen as the extraction buffer. The surfactants in the extraction buffer, serve to both lyse the virus if any is present and help reduce non-specific binding of proteins and secondary antibodies to the test line. Additionally, all components of extraction buffer are diluted in 1.5× peroxide buffer, which provides peroxide to HRP to facilitate the enzymatic reaction. The volume of TMB dried on the conjugate release pads was determined by holding all other conditions constant and adjusting the TMB volume. Volume was used for optimization instead of concentration as the concentration is proprietary information from the supplier. The buffer conditions described above were used, and the MM05-HRP concentration was 20 μg/mL. Devices were then run at 0 and 550 PFU/mL for each TMB volume. A volume of 22.5 μL was chosen as the condition that gave the greatest signal before increasing signal in the blanks (Fig. 3A). The concentration of MM05-HRP was determined in a similar fashion. All other conditions were held constant, and the concentration of the 2°Ab-HRP was varied. For the 2°Ab-HRP, 5 μL of 20 μg/mL was chosen similar reasons as the TMB optimization. Despite the large error in the positives, 20 μg/mL MM05-HRP is the concentration that had the greatest average signal before increasing the error (caused by false positives) in the blank (Fig. 3A and B).

3.1. Assay performance

Fig. 4 shows the comparison between the CaDI device and a well-plate ELISA using inactivated SARS-CoV-2 spiked into extraction buffer. Here, analytical LODs (Eqs. S2 and S3) of 8 and 84 PFU/mL were determined for the well plate ELISA and CaDI device, respectively. Although this is a 10-fold difference in LOD, the four parameter logistic fits for these curves align closely, but the biggest contribution affecting the LOD is the standard deviation of the blank. The higher LOD and greater standard deviation is due in part to the difference in the instrumentation used for quantification: A UV–Vis spectrophotometer with a 0.5 cm path length for the well-plate ELISA versus a cell phone image inside a homemade light box for the CaDI. Additionally, the TMB solution used here is supposed to make an insoluble product that will remain at the test line; however, some oxidized TMB is observed flowing into the waste pad. In the well-plate ELISA, all the product is contained in the well, ensuring all colored product is detected by the plate reader. Importantly, the CaDI device achieved similar performance to the ELISA in a much simpler format. The well-plate ELISA requires 18 pipetting steps, over 5 h of analysis time, and an expensive instrument for quantification. The CaDI only requires one pipetting step, 15 min from sample addition to result, and results can be quantified from smartphone images. Despite these differences in equipment, LOD, and standard deviation, the results in Fig. 4 demonstrate the CaDI device's ability to

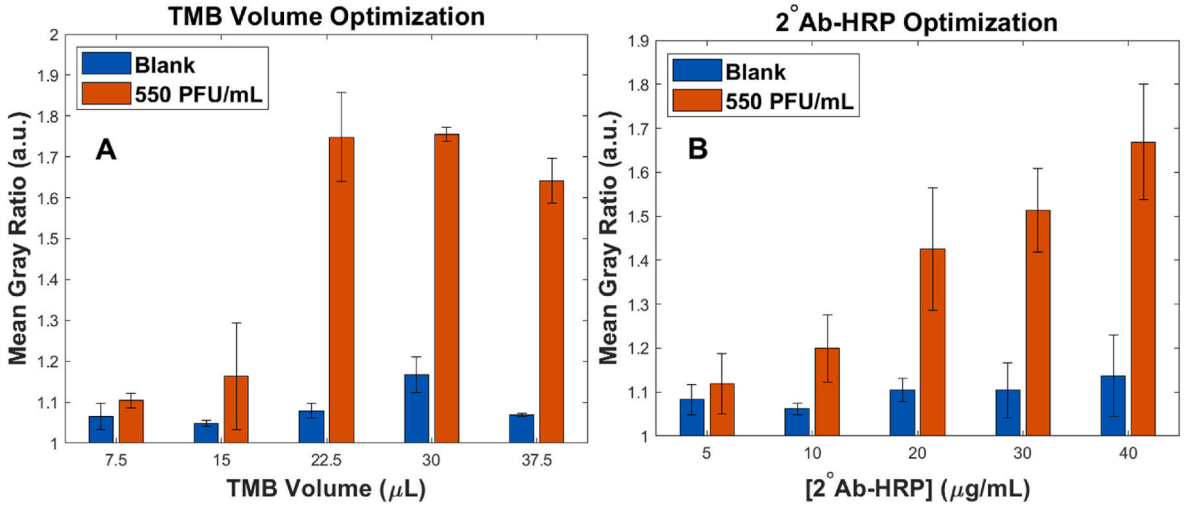

Fig. 3. (A) Buffer conditions and 2°Ab-HRP concentrations were held constant (20 μg/mL) while the volume of TMB dried on the conjugate release pad was varied. (B) Buffer conditions and TMB volume were held constant (22.5 μL) while the concentration of 2°Ab-HRP was varied. Each condition was run with 0 and 550 PFU/mL of inactivated virus to determine the condition that would give the greatest signal without increasing the signal of the blank.

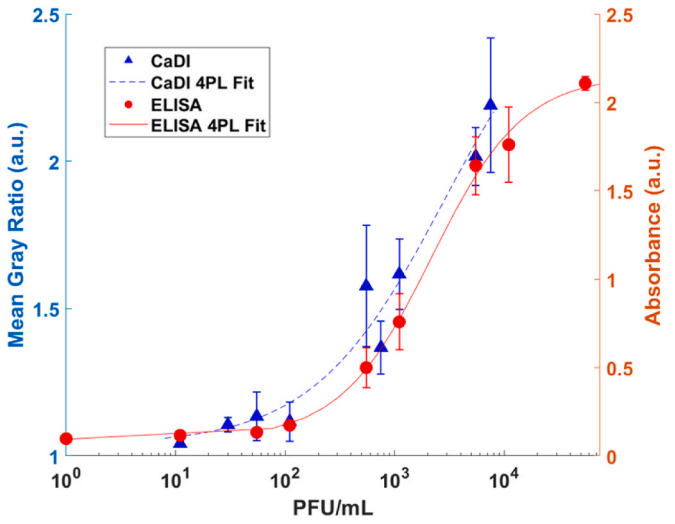

Fig. 4. Inactivated virus diluted in extraction buffer comparing the CaDI devices (blue triangles and dashed trace) to a well-plate ELISA (red circles and solid trace). The limits of detection were 86 PFU/mL and 8 PFU/mL for the CaDI and ELISA respectively. Each point for the well-plate ELISA and CaDI devices were run as n = 3 for standard deviation, except for the blank in the CaDI devices which was run as n = 5. (For interpretation of the references to color in this figure legend, the reader is referred to the Web version of this article.)

provide similar performance of a complex, laboratory-based ELISA with the simplicity of a standard LFA. Previous work using electrochemical detection for SARS-CoV-2 obtained a LOD of 68 PFU/mL, on the same order of magnitude of the results obtained in this work [51]. Further optimization can be done to improve the LOD and standard deviation further, but because the most likely use-case of the CaDI device in its current form would be a qualitative, positive/negative readout for an end user, the error at higher virus concentrations is acceptable.

3.2. Nasal swab samples

To demonstrate the CaDI device's ability to perform in complex sample matrices, spiked nasal swab samples were also run in the device. Unfortunately, due to cellular debris and mucins from nasal samples, the pores of the nitrocellulose clog in the current design of the device, so a filtering step was implemented for nasal swab samples. This filtering step is necessary for the current device format, but future work will incorporate on-device filtering to maintain simplicity for POC testing. Anterior nares nasal swab samples were collected from individuals who had recently tested negative for SARS-CoV-2, andvarying inactivated virus concentrations was added to the swab. Swabs were submerged in extraction buffer, filtered, and sample was added to the CaDI device sample inlet. After filtering, the nasal sample assays completed in a similar amount of time as the assays run with buffer (15–20 min). Two types of detection limit were determined using contrived nasal swab samples. First, an analytical LOD of 222 PFU/mL of the solution spiked on the nasal swab was determined (Fig. 5) using smartphone images and image processing described above. This LOD is slightly more than double that of the virus diluted in extraction buffer. This increased LOD can be accounted for considering that 50 μL of virus sample initially spiked onto a swab is diluted in 300 μL of buffer. It is possible that the sample matrix complexity and loss to the swab and filter also

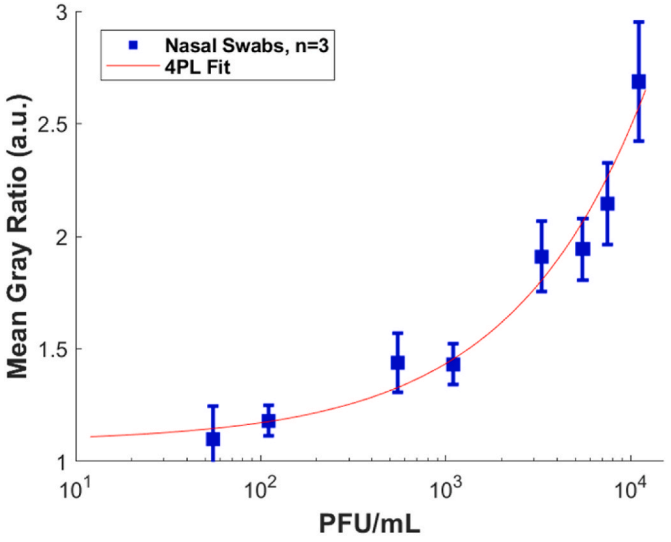

Fig. 5. 50 μL of varying virus concentrations was added to nasal swabs after collected (n = 3 for each concentration). The swabs were submerged in extraction buffer, filtered, and added to the device. The LOD from this study was 222 PFU/mL.

contributed to the higher LOD.

Although the image collection and data processing are relatively simple for the nasal swab sample LOD above, an end-user would not be expected to perform that quantitative analysis. Therefore, the most likely use case for a colorimetric detection for at-home, low-resource, or POC diagnostics would be a qualitative, yes/no visual determination. To this end, a visual LOD was determined following the FDA's protocol [59]. Anterior nares swab samples were collected and spiked with six varying inactivated virus concentrations. The same swab sample procedure described above was used, and sample was added to CaDI devices. The resulting nitrocellulose strips were shown in random order to 20 untrained end-users who were blinded to the virus concentration. Individuals were asked to identify which strips were positive, e.g., which strips showed both test and control lines. Of the individuals polled, 100% identified 100 PFU/mL as positive, and 0% identified the blank as positive (Table 1). The FDA suggests that a visual LOD is the concentration at which 19/20 untrained end users can correctly identify a positive result (95% sensitivity) [59], meaning the visual LOD for the CaDI is 100 PFU/mL from this study. This LOD is significantly below commercial tests on the market today [16].

Table 1
Visual limit of detection study. Twenty individuals were asked to identify positive results on nitrocellulose that was run from nasal swabs with the virus concentrations listed below.

Virus Concentration (PFU/mL)	0	50	100[a]	200	300	400	500
Individuals who marked "positive"	0	7	20	20	20	20	20
Total individuals polled	20	20	20	20	20	20	20
Percent correctly identified	100%	35%	100%	100%	100%	100%	100%

[a] Visual LOD.

4. Conclusion

Current antigen LFA devices, while easy to use and relatively cost effective, are limited in specificity and sensitivity due to the lack of signal amplification and washing steps. An ideal replacement would maintain the operational simplicity of LFAs while adding these functions found in more sophisticated ELISA assays. The CaDI device in this work addresses the shortcomings of current LFA technologies by adding a microfluidic front end to provide complicated fluid handling in line with a nitrocellulose membrane. While previous versions of this assay use electrochemical detection and expensive potentiostats to quantify results, the assay performed in this work can be read visually or with a smartphone, making it affordable and accessible to potential end users. Using the CaDI device, we were able to quantify clinically relevant levels of SARS-CoV-2 *N*-protein from nasal swabs in under 20 min with smartphone images. Furthermore, we were able to show detection limits of 100 PFU/mL for contrived nasal swab samples using naked eye detection by untrained users. This represents a significant improvement over existing COVID-19 LFA systems. In the future, we plan on testing the robustness of the system out of the lab, including tolerance testing for climate, sample volume variations, and manufacturing errors. Finally, while the CaDI device has been used to detect SARS-CoV-2, by changing the antibodies and antigens used in the device, we can detect any biomarker(s) associated with other disease states. Due to its low cost and ease of use, we believe the CaDI device will be a valuable platform for rapid diagnostics in the future.

CRediT authorship contribution statement

Jeremy S. Link: Conceptualization, Methodology, Investigation, Formal analysis, Writing – original draft, Writing – review & editing. **Cody S. Carrell:** Conceptualization, Methodology, Investigation, Writing – original draft. **Ilhoon Jang:** Conceptualization, Methodology, Investigation, Writing – review & editing. **Elijah J.O. Barstis:** Investigation, Formal analysis, Writing – original draft. **Zachary D. Call:** Investigation. **Rae A. Bellows:** Investigation. **John J. Odonell-Sloan:** Investigation. **James S. Terry:** Investigation, Methodology, Resources, Writing – original draft. **Loran B.R. Anderson:** Investigation, Methodology, Resources, Writing – original draft. **Yosita Panraksa:** Investigation. **Brian J. Geiss:** Conceptualization, Project administration, Resources, Writing – review & editing, Funding acquisition. **David S. Dandy:** Conceptualization, Project administration, Resources, Writing – review & editing. **Charles S. Henry:** Conceptualization, Project administration, Resources, Writing – review & editing, Supervision, Funding acquisition.

Declaration of competing interest

The authors declare that they have no known competing financial interests or personal relationships that could have appeared to influence the work reported in this paper.

Data availability

Data will be made available on request.

Acknowledgements

Support for this work was provided by a grant from the National Institute of Health through the SPARK-REACH program (UO1-HL152405) and through R01AI132668 and R01EB031510. Additional support was provided by the National Science Foundation (NSF STTR 2032222).

Appendix A. Supplementary data

Supplementary data to this article can be found online at https://doi.org/10.1016/j.aca.2023.341634.

References

[1] X. He, E.H.Y. Lau, P. Wu, X. Deng, J. Wang, X. Hao, Y.C. Lau, J.Y. Wong, Y. Guan, X. Tan, X. Mo, Y. Chen, B. Liao, W. Chen, F. Hu, Q. Zhang, M. Zhong, Y. Wu, L. Zhao, F. Zhang, B.J. Cowling, F. Li, G.M. Leung, Temporal dynamics in viral shedding and transmissibility of COVID-19, Nat. Med. 26 (5) (2020) 672–675.
[2] M. Cevik, M. Tate, O. Lloyd, A.E. Maraolo, J. Schafers, A. Ho, SARS-CoV-2, SARS-CoV, and MERS-CoV viral load dynamics, duration of viral shedding, and infectiousness: a systematic review and meta-analysis, The Lancet Microbe 2 (1) (2021) e13–e22.
[3] M. Cevik, K. Kuppalli, J. Kindrachuk, M. Peiris, Virology, transmission, and pathogenesis of SARS-CoV-2, BMJ 371 (2020), m3862.
[4] M.E. Kretzschmar, G. Rozhnova, M.C.J. Bootsma, M. van Boven, J.H.H.M. van de Wijgert, M.J.M. Bonten, Impact of delays on effectiveness of contact tracing strategies for COVID-19: a modelling study, Lancet Public Health 5 (8) (2020) e452–e459.
[5] O. Vandenberg, D. Martiny, O. Rochas, A. van Belkum, Z. Kozlakidis, Considerations for diagnostic COVID-19 tests, Nat. Rev. Microbiol. 19 (3) (2021) 171–183.
[6] S. Pickering, R. Batra, B. Merrick, L.B. Snell, G. Nebbia, S. Douthwaite, F. Reid, A. Patel, M.T. Kia Ik, B. Patel, T. Charalampous, A. Alcolea-Medina, M.J. Lista, P. R. Cliff, E. Cunningham, J. Mullen, K.J. Doores, J.D. Edgeworth, M.H. Malim, S.J. D. Neil, R.P. Galão, Comparative performance of SARS-CoV-2 lateral flow antigen tests and association with detection of infectious virus in clinical specimens: a single-centre laboratory evaluation study, The Lancet Microbe 2 (9) (2021) e461–e471.
[7] N. Toropov, E. Osborne, L.T. Joshi, J. Davidson, C. Morgan, J. Page, J. Pepperell, F. Vollmer, SARS-CoV-2 tests: bridging the gap between laboratory sensors and clinical applications, ACS Sens. 6 (8) (2021) 2815–2837.
[8] S. Alexandersen, A. Chamings, T.R. Bhatta, SARS-CoV-2 genomic and subgenomic RNAs in diagnostic samples are not an indicator of active replication, Nat. Commun. 11 (1) (2020) 6059.
[9] D.B. Larremore, B. Wilder, E. Lester, S. Shehata, J.M. Burke, J.A. Hay, M. Tambe, M.J. Mina, R. Parker, Test sensitivity is secondary to frequency and turnaround time for COVID-19 screening, Sci. Adv. 7 (1) (2021) eabd5393.

[10] M.J. Mina, R. Parker, D.B. Larremore, Rethinking Covid-19 Test Sensitivity — A Strategy for Containment, N. Engl. J. Med. 383 (22) (2020), e120.

[11] E.T. Chin, B.Q. Huynh, L.A.C. Chapman, M. Murrill, S. Basu, N.C. Lo, Frequency of routine testing for Coronavirus Disease 2019 (COVID-19) in high-risk healthcare environments to reduce outbreaks, Clin. Infect. Dis. 73 (9) (2020) e3127–e3129.

[12] A.D. Paltiel, A. Zheng, R.P. Walensky, Assessment of SARS-CoV-2 screening strategies to permit the safe reopening of college campuses in the United States, JAMA Netw. Open 3 (7) (2020), e2016818. -e2016818.

[13] A. St John, C.P. Price, Existing and emerging technologies for point-of-care testing, Clin. Biochem. Rev. 35 (3) (2014) 155–167.

[14] Z. Igloi, J. Velzing, J. van Beek, D. van de Vijver, G. Aron, R. Ensing, K. Benschop, W. Han, T. Boelsums, M. Koopmans, C. Geurtsvankessel, R. Molenkamp, Clinical evaluation of roche SD biosensor rapid antigen test for SARS-CoV-2 in municipal Health service testing site, The Netherlands, Emerg. Infect. Dis. J. 27 (5) (2021) 1323.

[15] A. Fernandez-Montero, J. Argemi, J.A. Rodríguez, A.H. Ariño, L. Moreno-Galarraga, Validation of a rapid antigen test as a screening tool for SARS-CoV-2 infection in asymptomatic populations. Sensitivity, specificity and predictive values, eClinicalMed. 37 (2021).

[16] A.I. Cubas-Atienzar, K. Kontogianni, T. Edwards, D. Wooding, K. Buist, C. R. Thompson, C.T. Williams, E.I. Patterson, G.L. Hughes, L. Baldwin, C. Escadafal, J.A. Sacks, E.R. Adams, Limit of detection in different matrices of 19 commercially available rapid antigen tests for the detection of SARS-CoV-2, Sci. Rep. 11 (1) (2021), 18313.

[17] S. Jegerlehner, F. Suter-Riniker, P. Jent, P. Bittel, M. Nagler, Diagnostic accuracy of a SARS-CoV-2 rapid antigen test in real-life clinical settings, Int. J. Infect. Dis. 109 (2021) 118–122.

[18] C. Jeewandara, D. Guruge, P.D. Pushpakumara, D. Madhusanka, T.T. Jayadas, I. P. Chaturanga, I.S. Aberathna, S. Danasekara, T. Pathmanathan, D. Jayathilaka, G. Somathilaka, H. Kuruppu, L. Gomes, V. Gunasekara, R. Wijayamuni, G.S. Ogg, G.N. Malavige, Sensitivity and specificity of two WHO approved SARS-CoV2 antigen assays in detecting patients with SARS-CoV2 infection, BMC Infect. Dis. 22 (1) (2022) 276.

[19] J. Dinnes, J.J. Deeks, A. Adriano, S. Berhane, C. Davenport, S. Dittrich, D. Emperador, Y. Takwoingi, J. Cunningham, S. Beese, J. Dretzke, L. Ferrante di Ruffano, I.M. Harris, M.J. Price, S. Taylor-Phillips, L. Hooft, M.M. Leeflang, R. Spijker, A. Van den Bruel, Rapid, point-of-care antigen and molecular-based tests for diagnosis of SARS-CoV-2 infection, Cochrane Database Syst. Rev. 8 (8) (2020), Cd013705.

[20] Antigen-detection in the diagnosis of SARS-CoV-2 infection. https://www.who.int/publications/i/item/antigen-detection-in-the-diagnosis-of-sars-cov-2infection-using-rapid-immunoassays. (Accessed 6 December 2022).

[21] C.-M. Cheng, A.W. Martinez, J. Gong, C.R. Mace, S.T. Phillips, E. Carrilho, K. A. Mirica, G.M. Whitesides, Paper-based ELISA, Angew. Chem. Int. Ed. 49 (28) (2010) 4771–4774.

[22] C.-K. Hsu, H.-Y. Huang, W.-R. Chen, W. Nishie, H. Ujiie, K. Natsuga, S.-T. Fan, H.-K. Wang, J.Y.-Y. Lee, W.-L. Tsai, H. Shimizu, C.-M. Cheng, Paper-based ELISA for the detection of autoimmune antibodies in body fluid—the case of bullous pemphigoid, Anal. Chem. 86 (9) (2014) 4605–4610.

[23] L. Ma, A. Nilghaz, J.R. Choi, X. Liu, X. Lu, Rapid detection of clenbuterol in milk using microfluidic paper-based ELISA, Food Chem. 246 (2018) 437–441.

[24] S. Kim, Y. Hao, E.A. Miller, D.M.Y. Tay, E. Yee, P. Kongsuphol, H. Jia, M. McBee, P. R. Preiser, H.D. Sikes, Vertical flow cellulose-based assays for SARS-CoV-2 antibody detection in human serum, ACS Sens. 6 (5) (2021) 1891–1898.

[25] H. Jia, E.A. Miller, C.C. Chan, S.Y. Ng, M. Prabakaran, M. Tao, I.S.-Y. Cheong, S. M. Lim, M.W. Chen, X. Gao, A. R, M.E. McBee, P.R. Preiser, H.D. Sikes, P. Kongsuphol, Development and translation of a paper-based top readout vertical flow assay for SARS-CoV-2 surveillance, Lab Chip 22 (7) (2022) 1321–1332.

[26] M.S. Verma, M.-N. Tsaloglou, T. Sisley, D. Christodouleas, A. Chen, J. Milette, G. M. Whitesides, Sliding-strip microfluidic device enables ELISA on paper, Biosens. Bioelectron. 99 (2018) 77–84.

[27] C.-A. Chen, W.-S. Yeh, T.-T. Tsai, C.-F. Chen, Three-dimensional origami paper-based device for portable immunoassay applications, Lab Chip 19 (4) (2019) 598–607.

[28] S. Huang, K. Abe, S. Bennett, T. Liang, P.D. Ladd, L. Yokobe, C.E. Anderson, K. Shah, J. Bishop, M. Purfield, Disposable autonomous device for swab-to-result diagnosis of influenza, Anal. Chem. 89 (11) (2017) 5776–5783.

[29] A. Apilux, Y. Ukita, M. Chikae, O. Chailapakul, Y. Takamura, Development of automated paper-based devices for sequential multistep sandwich enzyme-linked immunosorbent assays using inkjet printing, Lab Chip 13 (1) (2013) 126–135.

[30] J. Zhang, X. Gui, Q. Zheng, Y. Chen, S. Ge, J. Zhang, N. Xia, An HRP-labeled lateral flow immunoassay for rapid simultaneous detection and differentiation of influenza A and B viruses, J. Med. Virol. 91 (3) (2019) 503–507.

[31] C.S. Carrell, R.M. Wydallis, M. Bontha, K.E. Boehle, J.R. Beveridge, B.J. Geiss, C. S. Henry, Rotary manifold for automating a paper-based Salmonella immunoassay, RSC Adv. 9 (50) (2019) 29078–29086.

[32] H. Ordutowski, F. Dal Dosso, W. De Wispelaere, C. Van Tricht, S. Vermeire, N. Geukens, A. Gils, D. Spasic, J. Lammertyn, Next generation point-of-care test for therapeutic drug monitoring of adalimumab in patients diagnosed with autoimmune diseases, Biosens. Bioelectron. 208 (2022), 114189.

[33] M. Yafia, O. Ymbern, A.O. Olanrewaju, A. Parandakh, A. Sohrabi Kashani, J. Renault, Z. Jin, G. Kim, A. Ng, D. Juncker, Microfluidic chain reaction of structurally programmed capillary flow events, Nature 605 (7910) (2022) 464–469.

[34] A.P. Iakovlev, A.S. Erofeev, P.V. Gorelkin, Novel pumping methods for microfluidic devices: a comprehensive review, Biosensors 12 (11) (2022) 956.

[35] S.U. Hassan, X. Zhang, Design and fabrication of capillary-driven flow device for point-of-care diagnostics, Biosensors 10 (4) (2020).

[36] M. Ji, Y. Xia, J.F.-C. Loo, L. Li, H.-P. Ho, J. He, D. Gu, Automated multiplex nucleic acid tests for rapid detection of SARS-CoV-2, influenza A and B infection with direct reverse-transcription quantitative PCR (dirRT-qPCR) assay in a centrifugal microfluidic platform, RSC Adv. 10 (56) (2020) 34088–34098.

[37] F. Tian, C. Liu, J. Deng, Z. Han, L. Zhang, Q. Chen, J. Sun, A fully automated centrifugal microfluidic system for sample-to-answer viral nucleic acid testing, Sci. China Chem. 63 (10) (2020) 1498–1506.

[38] M.R. Jamiruddin, B.A. Meghla, D.Z. Islam, T.A. Tisha, S.S. Khandker, M. U. Khondoker, M.A. Haq, N. Adnan, M. Haque, Microfluidics technology in SARS-CoV-2 diagnosis and beyond: a systematic review, Life 12 (5) (2022).

[39] K.-L. Ho, H.-Y. Liao, H.M. Liu, Y.-W. Lu, P.-K. Yeh, J.Y. Chang, S.-K. Fan, Digital microfluidic qPCR cartridge for SARS-CoV-2 detection, Micromachines 13 (2) (2022) 196.

[40] V. Jain, K. Muralidhar, Electrowetting-on-Dielectric system for COVID-19 testing, Transac. Ind. Nat. Acad. Eng. 5 (2) (2020) 251–254.

[41] E. Fu, T. Liang, P. Spicar-Mihalic, J. Houghtaling, S. Ramachandran, P. Yager, Two-dimensional paper network format that enables simple multistep assays for use in low-resource settings in the context of malaria antigen detection, Anal. Chem. 84 (10) (2012) 4574–4579.

[42] G.E. Fridley, H. Le, P. Yager, Highly sensitive immunoassay based on controlled rehydration of patterned reagents in a 2-dimensional paper network, Anal. Chem. 86 (13) (2014) 6447–6453.

[43] B.J. Toley, B. McKenzie, T. Liang, J.R. Buser, P. Yager, E. Fu, Tunable-delay shunts for paper microfluidic devices, Anal. Chem. 85 (23) (2013) 11545–11552.

[44] J.H. Shin, J. Park, S.H. Kim, J.-K. Park, Programmed sample delivery on a pressurized paper, Biomicrofluidics 8 (5) (2014), 054121.

[45] J. Park, J.-K. Park, Pressed region integrated 3D paper-based microfluidic device that enables vertical flow multistep assays for the detection of C-reactive protein based on programmed reagent loading, Sensor. Actuator. B Chem. 246 (2017) 1049–1055.

[46] R.B. Channon, M.P. Nguyen, A.G. Scorzelli, E.M. Henry, J. Volckens, D.S. Dandy, C. S. Henry, Rapid flow in multilayer microfluidic paper-based analytical devices, Lab Chip 18 (5) (2018) 793–802.

[47] I. Jang, H. Kang, S. Song, D.S. Dandy, B.J. Geiss, C.S. Henry, Flow control in a laminate capillary-driven microfluidic device, Analyst 146 (6) (2021) 1932–1939.

[48] I. Jang, D.B. Carrão, R.F. Menger, A.R. Moraes de Oliveira, C.S. Henry, Pump-free microfluidic rapid mixer combined with a paper-based channel, ACS Sens. 5 (7) (2020) 2230–2238.

[49] Z.D. Call, C.S. Carrell, I. Jang, B.J. Geiss, D.S. Dandy, C.S. Henry, Paper-based pump-free magnetophoresis, Anal. Methods 12 (43) (2020) 5177–5185.

[50] J. Ilhoon, S.D. David, J.G. Brian, H. Charles, K. Hyunwoong, S. Simon, Flow Control in a Laminate Capillary-Driven Microfluidic Device, 2020.

[51] K.M. Clark, M.S. Schenkel, T.W. Pittman, I.C. Samper, L.B.R. Anderson, W. Khamcharoen, S. Elmegerhi, R. Perera, W. Siangproh, A.J. Kennan, B.J. Geiss, D.S. Dandy, C.S. Henry, Electrochemical capillary driven immunoassay for detection of SARS-CoV-2, ACS Meas. Sci. Au 2 (6) (2022) 584–594.

[52] K. Krorakai, S. Klangphukhiew, S. Kulchat, R. Patramanon, Smartphone-based NFC potentiostat for wireless electrochemical sensing, Appl. Sci. 11 (1) (2021) 392.

[53] C. Carrell, I. Jang, J. Link, J.S. Terry, Z. Call, Y. Panraksa, O. Chailapakul, D. S. Dandy, B.J. Geiss, C.S. Henry, Capillary driven microfluidic sequential flow device for point-of-need ELISA: COVID-19 serology testing, Anal. Methods: Adv. Methods Appl. 15 (22) (2023) 2721–2728.

[54] Y. Panraksa, I. Jang, C.S. Carrell, A.G. Amin, O. Chailapakul, D. Chatterjee, C. S. Henry, Simple manipulation of enzyme-linked immunosorbent assay (ELISA) using an automated microfluidic interface, Anal. Methods 14 (18) (2022) 1774–1781.

[55] S. Ramachandran, E. Fu, B. Lutz, P. Yager, Long-term dry storage of an enzyme-based reagent system for ELISA in point-of-care devices, Analyst 139 (6) (2014) 1456–1462.

[56] J.S. Terry, L.B.R. Anderson, M.S. Scherman, C.E. McAlister, R. Perera, T. Schountz, B.J. Geiss, Development of a SARS-CoV-2 nucleocapsid specific monoclonal antibody, Virology 558 (2021) 28–37.

[57] C.S. Carrell, R.M. Wydallis, M. Bontha, K.E. Boehle, J.R. Beveridge, B.J. Geiss, C. S. Henry, Rotary manifold for automating a paper-based Salmonella immunoassay, RSC Adv. 9 (50) (2019) 29078–29086.

[58] K.E. Boehle, E. Doan, S. Henry, J.R. Beveridge, Sangmi L. Pallickara, C.S. Henry, Single board computing system for automated colorimetric analysis on low-cost analytical devices, Anal. Methods 10 (44) (2018) 5282–5290.

[59] FDA in vitro diagnostics EUAs. https://www.fda.gov/medical-devices/coronavirus-disease-2019-covid-19-emergency-use-authorizations-medical-devices/vitro-diagnostics-euas. (Accessed 27 February 2021).

[60] G. Sapkal, A. Shete-Aich, R. Jain, P.D. Yadav, P. Sarkale, R. Lakra, S. Baradkar, G. R. Deshpande, D. Mali, B.N. Tilekar, T. Majumdar, H. Kaushal, Y. Gurav, N. Gupta, S. Mohandas, K. Deshpande, O. Kaduskar, M. Salve, S. Patil, S. Gaikwad, A. P. Sugunan, M. Ashok, S. Giri, J. Shastri, P. Abraham, R.R. Gangakhedkar, Covid Support Team: Pawar S, P. S. S. V. N. V. M. V. M. B. J. A. S. P. M. R. K. R. S. D. K., Development of indigenous IgG ELISA for the detection of anti-SARS-CoV-2 IgG, Indian J. Med. Res. 151 (5) (2020) 444–449.

[61] V. Roy, S. Fischinger, C. Atyeo, M. Slein, C. Loos, A. Balazs, C. Luedemann, M. G. Astudillo, D. Yang, D.R. Wesemann, R. Charles, A.J. Lafrate, J. Feldman, B. Hauser, T. Caradonna, T.E. Miller, M.R. Murali, L. Baden, E. Nilles, E. Ryan,

D. Lauffenburger, W.G. Beltran, G. Alter, SARS-CoV-2-specific ELISA development, J. Immunol. Methods 484–485 (2020), 112832.
[62] N.N. Hamidon, G.I. Salentijn, E. Verpoorte, Enhanced passive mixing for paper microfluidics, RSC Adv. 11 (41) (2021) 25677–25685.
[63] D.M. Cate, J.D. Bishop, H.V. Hsieh, V.A. Glukhova, L.F. Alonzo, H.G. Hermansky, B. Barrios-Lopez, B.D. Grant, C.E. Anderson, E. Spencer, S. Kuhn, R. Gallagher, R. Rivera, C. Bennett, S.A. Byrnes, J.T. Connelly, P.K. Dewan, D.S. Boyle, B. H. Weigl, K.P. Nichols, Antibody screening results for anti-nucleocapsid antibodies toward the development of a lateral flow assay to detect SARS-CoV-2 nucleocapsid protein, ACS Omega 6 (39) (2021) 25116–25123.

Further reading

[1] K.M. Koczula, A. Gallotta, Lateral flow assays, Essays Biochem. 60 (1) (2016) 111–120.
[2] S. Huang, K. Abe, S. Bennett, T. Liang, P.D. Ladd, L. Yokobe, C.E. Anderson, K. Shah, J. Bishop, M. Purfield, P.C. Kauffman, S. Paul, A.E. Welch, B. Strelitz, K. Follmer, K. Pullar, L. Sanchez-Erebia, E. Gerth-Guyette, G. Domingo, E. Klein, J.A. Englund, E. Fu, P. Yager, Disposable autonomous device for swab-to-result diagnosis of influenza, Anal. Chem. 89 (11) (2017) 5776–5783.